Feasibility of Multiplane-Transmit Beamforming for Real-Time Volumetric Cardiac Imaging: A Simulation Study

Yinran Chen, Ling Tong, *Member, IEEE*, Alejandra Ortega, *Student Member, IEEE*, Jianwen Luo, *Senior Member, IEEE*, and Jan D'hooge, *Member, IEEE*

***Abstract*— Today's 3-D cardiac ultrasound imaging systems suffer from relatively low spatial and temporal resolution, limiting their applicability in daily clinical practice. To address this problem, 3-D diverging wave imaging with spatial coherent compounding (DWC) as well as 3-D multiline-transmit (MLT) imaging have recently been proposed. Currently, the former improves the temporal resolution significantly at the expense of image quality and the risk of introducing motion artifacts, whereas the latter only provides a moderate gain in volume rate but mostly preserves quality. In this paper, a new technique for real-time volumetric cardiac imaging is proposed by combining the strengths of both approaches. Hereto, multiple planar (i.e., 2-D) diverging waves are simultaneously transmitted in order to scan the 3-D volume, i.e., multiplane transmit (MPT) beamforming. The performance of a 3MPT imaging system was contrasted to that of a 3-D DWC system and that of a 3-D MLT system by computer simulations during both static and moving conditions of the target structures while operating at similar volume rate. It was demonstrated that for stationary targets, the 3MPT imaging system was competitive with both the 3-D DWC and 3-D MLT systems in terms of spatial resolution and sidelobe levels (i.e., image quality). However, for moving targets, the image quality quickly deteriorated for the 3-D DWC systems while it remained stable for the 3MPT system while operating at twice the volume rate of the 3-D-MLT system. The proposed MPT beamforming approach was thus demonstrated to be feasible and competitive to state-of-the-art methodologies.**

***Index Terms*— 3-D ultrasound imaging, diverging wave beamforming, high frame rate, multiline transmit (MLT) beamforming, volumetric imaging.**

I. Introduction

THE 2-D echocardiography is a fundamental imaging modality in clinical practice to examine the heart as it offers advantages over other imaging techniques, such as low cost, easy operation, portability, and most importantly because of its real-time operation. The conventional single-line-transmit (SLT) method can achieve a frame rate of around 40 Hz, which is sufficient to capture the gross motion of the heart. As such, a series of cross-sectional views of the heart can be taken from different transducer positions allowing the cardiologist to make a clinical diagnosis. However, due to the 3-D nature of the heart, out-of-plane structures and motion are missed from 2-D imaging planes, complicating interpretation of the data. To overcome this limitation, 3-D echocardiography has been developed and plays an ever increasing role in clinical practice [1], [2]. However, it has not been fully adopted by clinicians because of its low spatiotemporal resolution as a result of the inherent tradeoff between image quality and frame rate in echocardiography.

Several techniques have been developed to increase the frame rate while trying to keep image quality acceptable. For instance, volume stitching is a method, where subvolumetric data taken at relatively high spatiotemporal resolution are acquired over several cardiac cycles through ECG gating and stitched to obtain a full volumetric image [3]. Although this strategy is adopted on most commercial scanners, it is often difficult or even impossible to perform on patients with heart rhythm disturbances.

As volume stitching in itself is not sufficient to obtain a 3-D image at acceptable spatiotemporal resolution, multiline acquisition (MLA) is another technique typically implemented on most high-end scanners resulting in a gain in frame rate equal to the number of MLA beams in the system [4]. In general, this technique requires to broaden the transmit beam, which can be done in multiple ways. Although originally the transducer's transmit aperture was reduced, more recently, plane wave or diverging wave transmits were proposed in order to allow for a large number of MLA beams [5]–[8]. Originally, these fast imaging approaches were proposed for 2-D imaging but very recently they were demonstrated to be extendable to 3-D [9], [10]. However, in order to avoid too much loss in image quality [i.e., spatial resolution and contrast-to-noise ratio (CNR)], spatial coherent compounding is typically needed thereby increasing the number of transmit events and compromising the effective gain in frame rate. Unfortunately, tissue motion during the compounding process can result in image artifacts in particular when a large number of compounds is used as in 3-D diverging wave imaging with spatial coherent compounding (DWC) (e.g., 9×9 compounds) [11], [12]. Finally, the use of unfocused

Manuscript received November 23, 2016; accepted January 6, 2017. Date of publication January 10, 2017; date of current version April 1, 2017. This work was supported in part by the European Research Council under the European Union's Seventh Framework Programme (FP7/2007-2013)/ERC under Grant 281748, in part by the National Natural Science Foundation of China under Grant 61271131 and Grant 61322101, and in part by the China National Postdoctoral Science Foundation under Grant 2014M560094. *(Corresponding authors: Jianwen Luo; Jan D'hooge.)*

Y. Chen and J. Luo are with the Department of Biomedical Engineering, School of Medicine, Tsinghua University, Beijing 100084, China (e-mail: luo_jianwen@tsinghua.edu.cn).

L. Tong was with the Department of Biomedical Engineering, School of Medicine, Tsinghua University, Beijing 100084, China. She is now with Supersonic Imagine, S.A., F-13857 AIX EN Provence, France.

A. Ortega and J. D'hooge are with the Laboratory on Cardiovascular Imaging and Dynamics, Department of Cardiovascular Sciences, Katholieke Universiteit Leuven, 3000 Leuven, Belgium (e-mail: jan.dhooge@uzleuven.be).

Digital Object Identifier 10.1109/TUFFC.2017.2651498

0885-3010 © 2017 IEEE. Personal use is permitted, but republication/redistribution requires IEEE permission.
See http://www.ieee.org/publications_standards/publications/rights/index.html for more information.

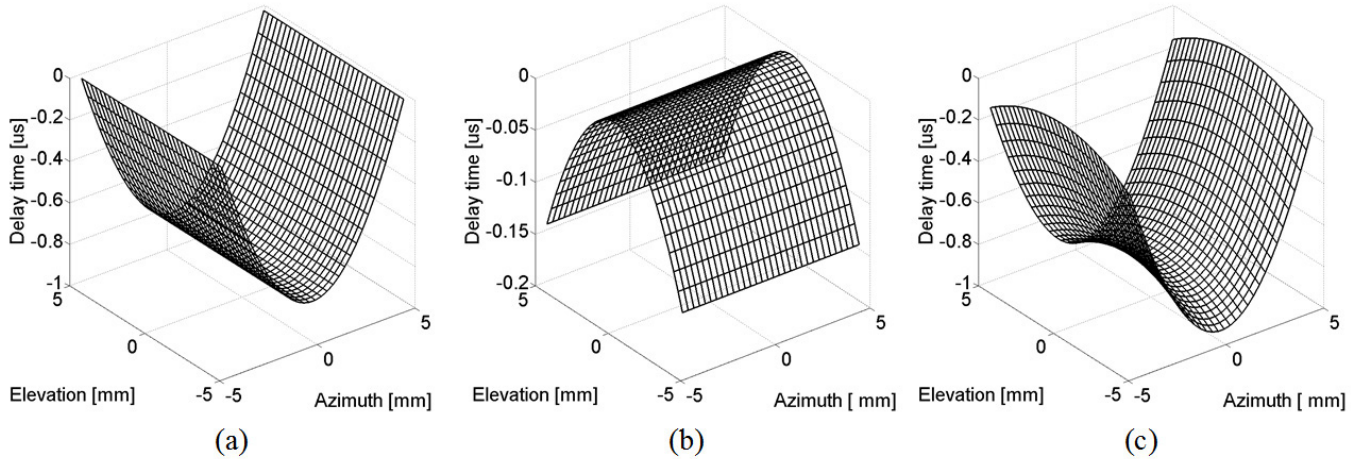

Fig. 1. Time delays of SPT for a 2-D matrix array transducer. (a) Transmit time delays for diverging wave component in the azimuth dimension. (b) Transmit time delays for focused wave component in the elevation dimension. (c) Summation of (a) and (b) for SPT time delays.

waves limits penetration depth, because the transmitted energy is spread over a larger region with direct impact on the signal-to-noise ratio (SNR) and as such velocity estimates [8].

As an alternative to MLA, multiple focused beams can simultaneously be transmitted into different directions [i.e., multiline transmit (MLT)] in order to increase the frame rate by a factor equal to the number of the MLT beams [13]–[15]. Recently, this technique has also been extended to 3-D, where it has shown promising results to generate high frame rate volumes while preserving image quality [16]–[18]. Although potential crosstalk artifacts due to the interference among MLT beams could arise, these artifacts can significantly be suppressed by properly positioning the MLT beams and/or adding apodization [14], [17], [18]. However, as a result of its line-by-line scanning nature, the frame rate of 3-D MLT system remains limited (∼32 Hz) [18], [19].

In this paper, we propose a hybrid beamforming approach to achieve fast 3-D cardiac ultrasound imaging. In particular, it is proposed to transmit multiple planar diverging waves [i.e., multiplane transmit (MPT)] simultaneously in 3-D space. In this way, the MPT beams are expected to behave as diverging waves in 1-D while they are focused in the orthogonal dimension and behave similar to MLT. The novelty of this paper therefore lies in the fusion of two state-of-the-art 3-D imaging methodologies with the ambition to exploit their relative strengths while mitigating their respective drawbacks.

This paper is organized as follows. First, the principle of MPT beamforming is explained and the feasibility of generating the required pressure fields is demonstrated. Then, the beam characteristics of a 3MPT imaging system are contrasted to those of a 9×9 DWC system, a 16MLT-4MLA system, and a conventional SLT-single-line-acquisition (SLA) system as a bench mark by computer simulations. Finally, the relative image quality of the proposed system is studied by simulating B-mode images and determining the point spread function (PSF), CNR, and its sensitivity to motion.

II. Methods

A. Principle of MPT Beamforming

For volumetric imaging, the use of a 3-D diverging wave has previously been proposed by making use of a virtual focus point behind the transducer [9], [10]. In order to generate a *planar* diverging wave using a 2-D matrix array, one needs to transmit a diverging wave in 1-D (e.g., azimuth), and a focused beam in the orthogonal dimension (e.g., elevation). For a linear system, the delays to generate such a single planar diverging wave [i.e., single-plane-transmit (SPT)] are simply the sum of the time delays required to generate a diverging wave in 1-D [see Fig. 1(a)] with the time delays required to generate a focused beam in the orthogonal direction [see Fig. 1(b)], as shown in Fig. 1(c). As such, the spatial location of the virtual source of the diverging wave and the focus depth of the focused beam are independent. Again assuming a linear system, simultaneously transmitting multiple planar diverging waves into different directions simply requires the superposition of multiple SPT beams focused at different directions in the elevation dimension similar to what is done for MLT imaging.

TABLE I
Transducer Configuration of the Matrix Array

Parameters	Values
Number of elements (azi × ele)	32 × 32
Element size	0.30 mm × 0.30 mm
Excitation pulse	Gaussian modulated cosine
Pulse center frequency	3.0 MHz
Pulse length	1.5 cycles
Pulse bandwidth	0.6
Sampling frequency	20 MHz
Transmit apodization	2-D Tukey ($\alpha = 0.5$)
Receive apodization	2-D Tukey ($\alpha = 0.5$)

azi = azimuth, ele = elevation.

B. Simulation Setup

A 32×32 element 2-D matrix array transmitting a Gaussian modulated cosine pulse with a central frequency of 3 MHz and 60% bandwidth was simulated in this paper. The transducer configuration parameters are given in Table I. Based on the previous findings [14], 2-D Tukey ($\alpha = 0.5$) windowing was applied in both transmit and receive apodizations to reduce

TABLE II
SETUP PARAMETERS OF DIFFERENT IMAGING SYSTEMS

Parameters	MPT imaging system	Contrasted imaging systems		
	3MPT	9 × 9 DWC	16MLT-4MLA	SLT-SLA
Opening angle (azi)	60°	60°	×	×
Opening angle (ele)	×	60°	×	×
Focus depth (azi)	×	×	50 mm	50 mm
Focus depth (ele)	50 mm	×	50 mm	50 mm
Number of compounds (azi)	5	9	×	×
Number of compounds (ele)	×	9	×	×
Number of MLT (azi)	×	×	4	1
Number of MLT (ele)	3	×	4	1
Tx sub-aperture size (azi × ele)	16 × 32	16 × 16	32 × 32	32 × 32
Rx sub-aperture size (azi × ele)	32 × 32	32 × 32	32 × 32	32 × 32
Pulse repetition frequency (PRF)	5133 Hz	5133 Hz	5133 Hz	5133 Hz
Frame rate (volumes / second)	34(SLA), 68(2MLA)	63	35	0.63

azi = azimuth, ele = elevation, Tx = transmit, Rx = receive

the potential crosstalk artifacts that might be introduced in the focused wave dimension. In receive, a 60° × 60° rectangular pyramidal volume was imaged up to 150-mm depth. In this volume, 90 × 90 image lines were reconstructed using a dynamically focused delay-and-sum approach. The speed of sound in all simulations was set to 1540 m/s while sampling was performed at 20 MHz. All simulations were performed in Field II [20]. Acoustic attenuation was not taken into account in this paper.

C. Feasibility of Generating a MPT Beam Profile

In order to investigate the feasibility of MPT beamforming, the pressure fields of a 1MPT (i.e., SPT) and a 3MPT system were simulated. Hereto, the opening angle of the planar diverging wave was set to 60° while the focus depth was put at 50 mm in the orthogonal dimension. The resulting pressure fields were estimated in a *C* plane at the focal position (i.e., 50 mm) as well as in planes in both the diverging wave and focused wave dimensions.

D. Imaging Systems Tested

To verify the quality of the beam profiles of the proposed MPT imaging with respect to state-of-the-art 3-D imaging methodologies, the following beamforming systems were simulated. Their schematic and detailed description are summarized in Fig. 2 and Table II, respectively.

1) 9 × 9 DWC: The system as described in [9] was simulated. Hereto, a 3-D diverging wave with an opening angle of 60° × 60° was transmitted sequentially from a virtual array of 9 × 9 sources located behind the probe using a transmit subaperture of 16 × 16 elements, as shown in Fig. 2(a) and (b). The 9 × 9 virtual sources placed with the intervals of two elements in the azimuth and elevation dimensions were transmitted one-by-one in an azimuth-major order (i.e., neighboring azimuthal virtual focus points are consecutively transmitted, see row-major matrices). Volumes were beamformed for every firing and subsequently coherently compounded to form a final volumetric image with relatively higher spatial resolution and higher CNR. The total number of firings was 81, leading to a frame rate of ∼63 volumes per second given a pulse repetition frequency (PRF) of 5133 Hz.

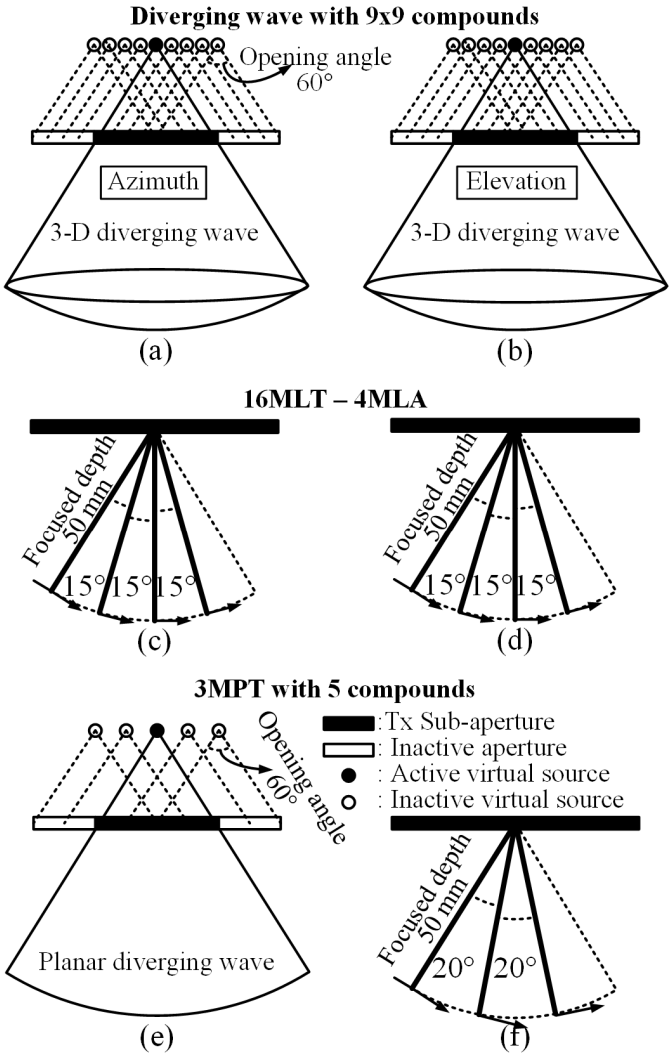

Fig. 2. Schematic of different 3-D beamforming systems. (a) and (b) 3-D diverging wave with 9 × 9 sources for spatial coherent compounding. (c) and (d) 16MLT-4MLA beamforming. (e) and (f) 3MPT imaging with five sources for spatial coherent compounding in the azimuth dimension, and three equidistant focused beams in the elevation dimension. Left: illustrations in the azimuth dimension. Right: elevation dimension.

2) 16MLT-4MLA: A system similar to the one described in [18] was simulated. Hereto, 16MLT beams were transmitted into four equidistant elevational planes (with an interplane

opening angle of 15°) with 4MLT beams equally spread in each of these planes (with an interbeam opening angle of 15°), as shown in Fig. 2(c) and (d). All MLT beams were focused at a depth of 50 mm. The transmit sequence was done in an azimuth-major order and for every firing, four image lines surrounding each of the MLT beams were reconstructed simultaneously (i.e., 4MLA). To generate a volume of 90 × 90 lines, 12 firings were needed in both dimensions, so the total number of firings was 144 and the resulting frame rate was ∼35 volumes per second.

3) 3MPT Imaging: Several aspects were taken into consideration when designing this imaging system. First, the number of coherent compounds in the diverging wave dimension and the number of MPT beams in the focused wave dimension should be carefully chosen in order to keep the spatial resolution and CNR in both dimensions similar thereby keeping image quality isotropic. Second, the angle between the neighboring MPT beams in the focused dimension should be relatively large in order to reduce potential crosstalk artifacts. Third, for a fair comparison, the frame rate should be competitive with alternative approaches (i.e., 63 volumes per second for 9×9 DWC and 35 volumes per second for 16MLT-4MLA, respectively.)

Taken the above criteria into account, five compounds were made in the diverging wave dimension with a 16-element transmit subaperture using a four elements interval, as shown in Fig. 2(e), while three equidistant MPT beams were placed in the orthogonal dimension with an interplane opening angle of 20°, as shown in Fig. 2(f). The MPT beams were diverging with 60° opening angle in the azimuth dimension and focused at 50-mm depth in the elevation dimension.

As such, the number of firings in the elevation dimension was 30 and the total firings to run the entire sequence was 150, leading to a frame rate of ∼34 volumes per second (i.e., 3MPT-SLA), competitive with the 16MLT-4MLA system. To achieve a higher frame rate, 2MLA was applied in the elevation dimension, implying that for every 3MPT firing, six image planes were reconstructed in parallel (i.e., 3MPT-2MLA). Thereby, the number of firings in the elevation dimension was halved resulting in a frame rate of ∼68 volumes per second, competitive with the 9 × 9 DWC system.

4) 3-D SLT-SLA Imaging: This imaging system was simulated as a bench mark. The transmit beam was focused at 50-mm depth and the full aperture was used for every transmit event. The focus points were evenly distributed on a spherical surface centered at the center of the transducer surface and with a radius of 50 mm. Receive beamforming was done line by line so that the time required to generate a single volume was around 1.58 s giving a frame rate of ∼0.63 volumes per second.

E. Quantification of Image Characteristics

In order to determine the PSF of the different 3-D imaging systems, four point scatterers were positioned on the symmetry axis of the volume from 20- to 110-mm depth with 30-mm spacing. The *C* planes through these scatterers were reconstructed in order to obtain the system PSF [see Fig. 3(a)] from which the azimuth and elevation resolutions were extracted at the −6-dB level. Moreover, the mean-sidelobe-level (MSLL) was estimated as the mean gray level outside the −6-dB isoline, as a predictor for the contrast performance of the respective imaging system.

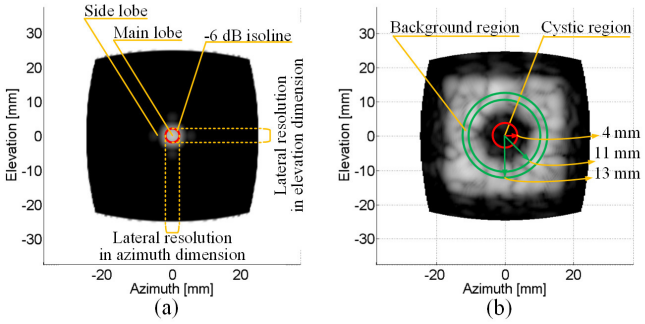

Fig. 3. Illustration of quantification of image characteristics. (a) Lateral profiles of the PSF. Region inside the red circle (i.e., −6-dB isoline): main lobe. Region outside the red circle: sidelobe. (b) B-mode image of the cystic phantom in a *C* plane. Red sphere: cystic region. Green spherical cell: background region.

Next, a tissue mimicking phantom was generated by positioning point scatterers at random positions at a density of 5/mm^3 in a cube of 30 mm × 30 mm × 40 mm (azimuth × elevation × axial) centered at a depth of 50 mm. A spheroidal cystic region with a radius of 10 mm was placed in the center of the cubic phantom by setting the scattering amplitude of these scatterers to 0 while for the remaining scatterers, this was uniformly distributed between 0 and 1. From this model, 3-D volumes were simulated with the respective imaging systems and the CNR of the resulting volumes was calculated as

$$\mathrm{CNR} = \frac{\mu_{\mathrm{dB\_back}} - \mu_{\mathrm{dB\_cyst}}}{\sqrt{\sigma^2_{\mathrm{dB\_cyst}} + \sigma^2_{\mathrm{dB\_back}}}} \tag{1}$$

where $\mu_{\mathrm{dB\_back}}$ and $\mu_{\mathrm{dB\_cyst}}$ were the mean gray level in the background and cystic regions, respectively, and $\sigma_{\mathrm{dB\_back}}$ and $\sigma_{\mathrm{dB\_cyst}}$ were their respective standard deviations. As shown in Fig. 3(b), the volume data inside a sphere with a radius of 4 mm were taken as the signal of the cystic region while a homocentric spherical cell outside the cystic region was selected as the background region. The internal and external radii of this spherical cell were 11 and 13 mm, respectively.

In addition to static imaging conditions, the above experiments were repeated for moving scatterers in the axial directions. The velocity was set to 5 cm/s in this direction as a realistic value for myocardial motion. To extract the CNR for these moving phantoms, the center of the sphere was relocated to the mean position of the motion path of the cyst over the whole acquisition period.

III. Results

A. Feasibility

Fig. 4(a) shows the pressure field profile of a 1MPT beam on a spherical surface (i.e., *C* plane) at a depth of 50 mm.

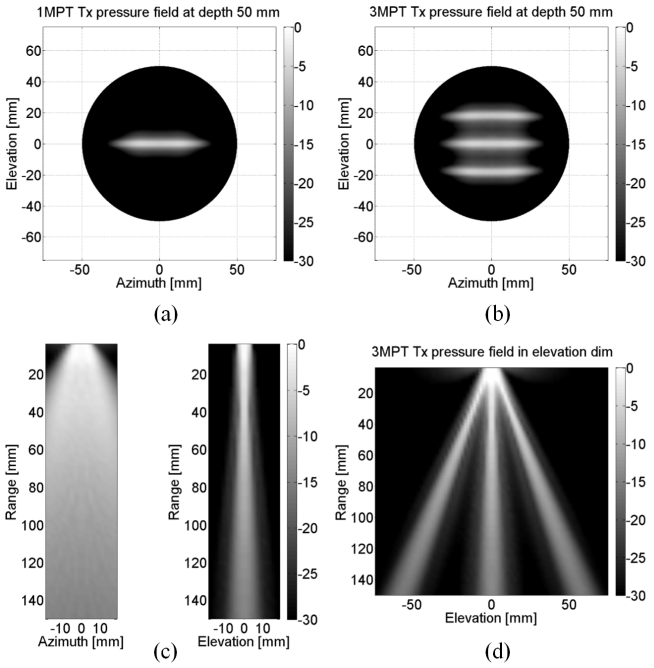

Fig. 4. Transmit pressure fields of a 1MPT and a 3MPT case. Three views of the 1MPT pressure field with (a) *C* plane and (c) orthogonal planes in the azimuth-axial and elevation-axial planes. (b) and (d) Views of the 3MPT pressure field. The opening angle of the diverging wave in the azimuth dimension is 60° and the focused depth is set at 50 mm in the elevation dimension.

The beam profiles of this configuration on orthogonal planes in the azimuth-axial and elevation-axial planes are shown in Fig. 4(c). Similarly, a *C* plane and the orthogonal plane in the elevation-axial plane (i.e., the focused wave dimension) for a 3MPT system are shown in Fig. 4(b) and (d), respectively. Generating a pressure field that behaves like a diverging wave in 1-D and an MLT system in the orthogonal dimension thus showed to be feasible.

B. PSFs for Static Targets

The PSFs of the four different 3-D imaging systems are presented in Fig. 5. The left column shows the 2-D image slices in the azimuth-axial plane, the middle column the elevation-axial plane, and the right column the *C* planes at the depths of each of the point scatterers. The PSF of the 9×9 DWC and 16MLT-4MLA were symmetric in both dimensions [see Fig. 5(f) and (l)]. However, for the 3MPT imaging systems (3MPT-2MLA and 3MPT-SLA), the PSF resembles that of the 9×9 DWC in the azimuth-axial plane while it looks like the PSF of the 16MLT-4MLA in the elevation-axial plane [see Fig. 5(c) and (i)].

Quantitative results of these PSFs are presented in Fig. 6. Fig. 6(a) and (b) shows the lateral resolution of the four point scatterers in the azimuth and elevation dimensions, respectively. PSF characteristics for the 9×9 DWC, the 16MLT-4MLA, and the SLT-SLA were—as expected—symmetric with the latter two systems having very competitive resolution. Similarly, the lateral resolution of both 3MPT systems was very competitive being better than that of the 9×9 DWC system but worse than that of the 16MLT-4MLA system. Importantly, as shown in Fig. 6(a) and (b), the lateral resolution of the 3MPT systems was closer to that of the 9×9 DWC system in the azimuth dimension (i.e., diverging wave dimension) while it was closer to that of the 16MLT-4MLA system in the elevation dimension (i.e., focused wave dimension).

The MSLL of the four point scatterers for the imaging systems tested is shown in Fig. 6(c), where the SLT-SLA system showed a spatially variant but the best MSLL with a minimal value at the focal depth (i.e., 50 mm). Both 3MPT imaging systems had similar MSLL values that were higher than that of the 9×9 DWC but lower than that of the 16MLT-4MLA.

C. Image Characteristics for Static Targets

Three orthogonal slices of the static phantom acquired with the 3MPT-2MLA, 9×9 DWC, 3MPT-SLA, and 16MLT-4MLA systems are presented in Fig. 7. Compared with the 9×9 DWC, the images of the 3MPT-2MLA system qualitatively showed more noise in the cystic region and outside the cubic phantom, which was consistent with the higher MSLL values [see Fig. 6(c)] and was confirmed quantitatively by a lower CNR value (6.80 versus 6.95, see Fig. 10). Meanwhile, the images of the 16MLT-4MLA system qualitatively showed more noise than those of the 3MPT-SLA system, which was also confirmed by higher MSLL values [see Fig. 6(c)] and a lower CNR value (5.58 versus 6.81, see Fig. 10). Please note that the CNR values of the two 3MPT systems were similar (i.e., 6.80 and 6.81 for the 3MPT-2MLA and 3MPT-SLA, respectively).

D. PSFs for Moving Targets

The effect of motion in the axial direction on the PSFs is shown in Fig. 8. In the comparison of 3MPT-2MLA and 9×9 DWC systems, the motion artifacts of the 9×9 DWC were severe particularly in the elevation dimension [see Fig. 8(e) and (f)]. On the contrary, the impact of axial motion on the PSF of the 3MPT-2MLA system remained limited, except that the PSFs became asymmetric due to the azimuth-major transmit sequence causing unequal time lags between sequential firings in the 2-D. As such, the longer time lags in the elevation dimension resulted in a small tilt of the PSF in this dimension [see Fig. 8(b) and (c)]. This latter effect was more pronounced for the 3MPT-SLA system [see Fig. 8(h)] given the increased elevational time lag for this sequence. Finally, the PSFs of the 16MLT-4MLA system in the azimuth dimension were doubled and in the elevational dimension were split, because the moving point scatterers were located on the border of the different MLT subsectors resulting in "stitching artifacts" for the implemented imaging sequence.

E. Image Characteristics for Moving Targets

Three orthogonal slices of the phantom images under axial motion are shown in Fig. 9. The motion resulted in stitching artifacts in the 3MPT-2MLA and 3MPT-SLA systems in the elevation dimension [see Fig. 9(b) and (h)]. For the 16MLT-4MLA system, similar stitching artifacts were found

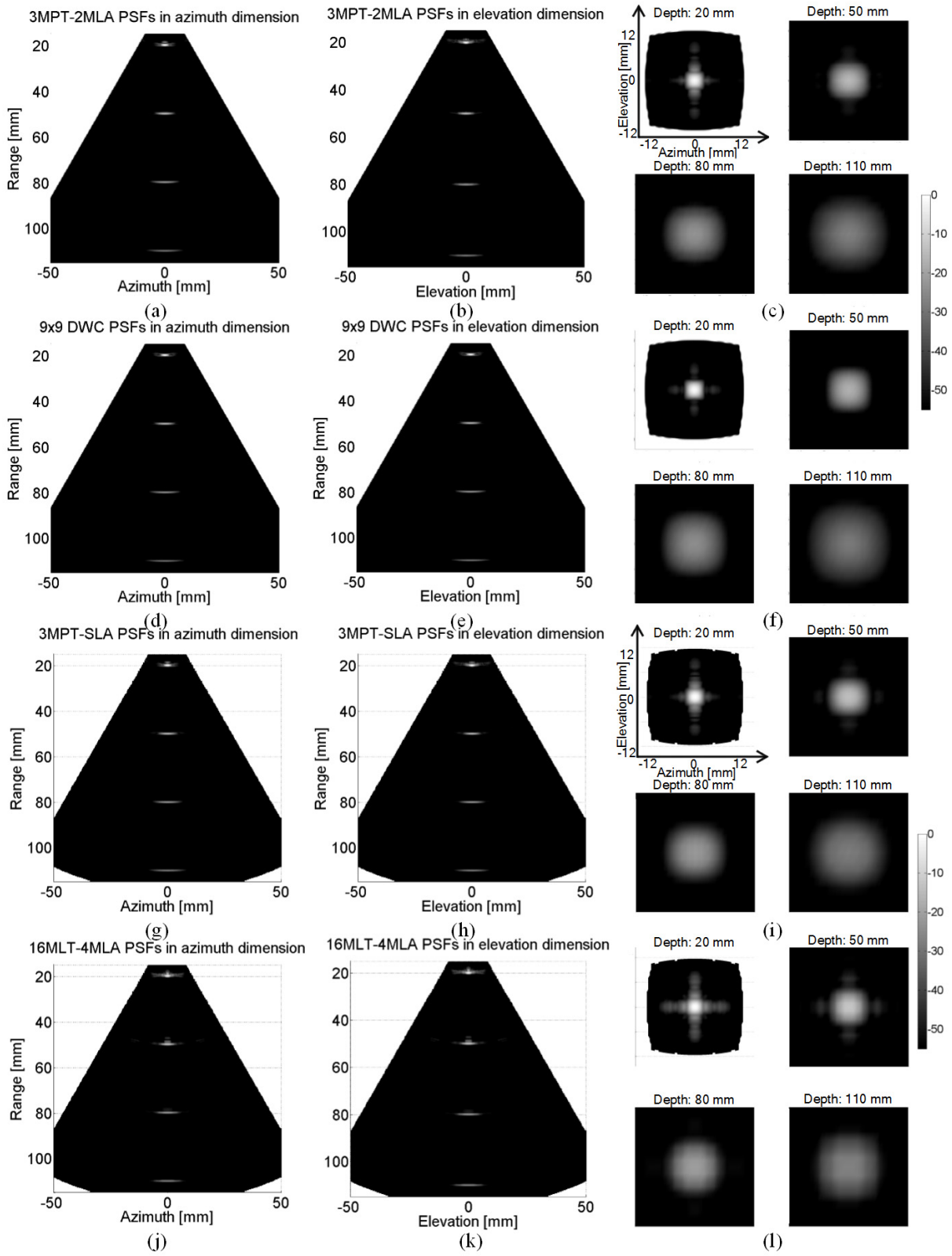

Fig. 5. PSF of different imaging systems. (a)–(c) Results of the 3MPT-2MLA. (d)–(f) 9 × 9 DWC. (g)–(i) 3MPT-SLA. (j)–(l) 16MLT-4MLA. Left: 2-D image slices in the azimuth-axial plane. Middle: elevation-axial plane. Right: *C* planes at the depths of each of the point scatterers. All the figures in the right column follow the same axes, as shown in the top-left one. The display dynamic range is −55 dB.

[see Fig. 9(k)]. These stitching artifacts were only present in the elevation dimension due to the azimuth-major transmit sequence leading to a longer time lag between image lines from adjacent subvolumes. For this reason, more severe stitching artifacts were expected in the 3MPT-SLA system compared with its 2MLA correlate as confirmed by the

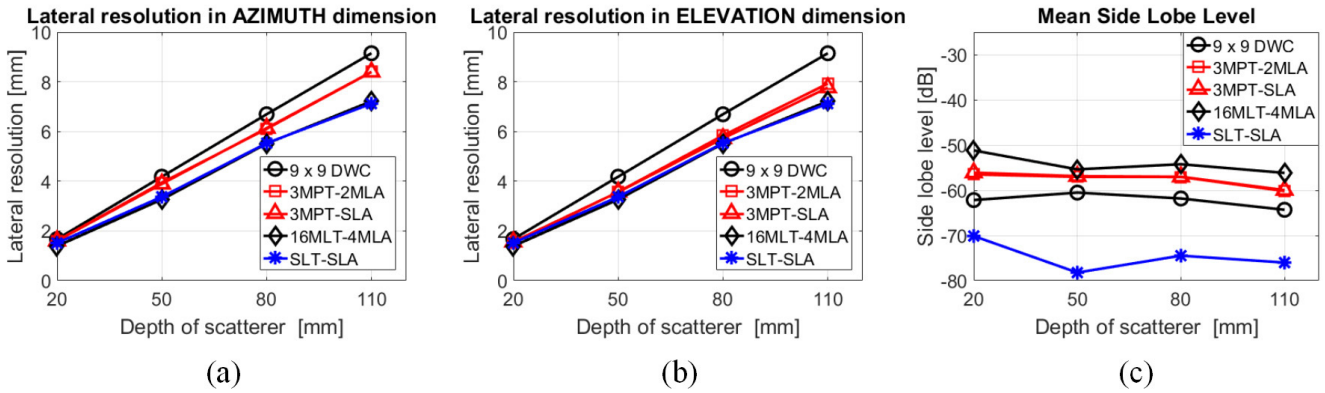

Fig. 6. Quantitative results of the PSFs shown in Fig. 5. (a) and (b) Lateral resolutions of the simulated imaging systems in the azimuth and elevation dimensions, respectively. (c) MSLL of the imaging systems. Please note that the quantitative results of the 3MPT-2MLA and 3MPT-SLA systems were almost overlapping.

simulated images [Fig. 9(b) and (h)]. The 9×9 DWC system showed a significant reduction in contrast, especially in the elevation dimension [see Fig. 9(d) and (e)]. This was confirmed quantitatively by its CNR, as shown in Fig. 10. As obvious from this figure, the 9×9 DWC had the best contrast performance when imaging a static object but was more sensitive to motion than any of the other fast imaging methodologies. Overall, the proposed 3MPT systems had the best CNR performance, as shown in Fig. 10.

IV. Discussion

In this study, we proposed MPT beamforming, which could be considered a linear combination of DWC and MLT in 3-D. When operating at competitive frame rate, it was demonstrated that the lateral resolution of the 3MPT systems outperforms that of their DWC correlate (i.e., 9×9 DWC), but remained worse than that of 16MLT-4MLA and SLT-SLA (see Fig. 6). In contrast, the MSLL obtained for the 3MPT systems was worse than that of the 9×9 DWC system but better than that of the 16MLT-4MLA system. These findings were confirmed by quantifying the CNR in simulated B-mode images (see Figs. 7 and 10). As such, the proposed MPT beamforming seems to provide a good compromise between the 16MLT-4MLA and the 9×9 DWC systems.

The fact that the MSLL was worse in the 3MPT systems than for 9×9 DWC is not surprising given that crosstalk between the parallel planar beams cannot completely be avoided despite the fact that transmit and receive Tukey ($\alpha = 0.5$) apodizations were used to suppress crosstalk artifacts. Yet, they performed better than the 16MLT-4MLA system given that interbeam angles in that setup were larger (i.e., 20° rather than 15°, see Fig. 2) thereby avoiding more crosstalk and worsening of the contrast performance [see Figs. 7 and 10]. Moreover, as the pressure waves from the simultaneously transmitted beams overlap in the near field (e.g., 20-mm depth), the MSLL of the corresponding point scatterer is particularly poor [see Fig. 6(c)]. Further reduction might be achieved by separating the MPT beams in the frequency domain [21], by using coded excitation [22], by introducing short time delays between the different MPT beams [23], or by aligning the parallel transmit directions along the transverse diagonal of the matrix array [17].

The effect of axial motion on both the PSFs and the CNR of the resulting images was minimal for the proposed 3MPT imaging systems (see Figs. 8–10). In contrast, due to the extensive compounding used in the 9×9 DWC, this system was very sensitive to axial motion, as it results in incoherence in the compounding process. More severe motion artifacts occurred in the elevation dimension in the 9×9 DWC system due to the azimuth-major transmit sequence, as this results in a nine times larger time lag of sequential firings in the elevation dimension than in the azimuth dimension. Importantly, motion artifacts were hardly observed in the azimuth dimension in the 3MPT systems even though coherent compounding was also used in this dimension (five virtual sources for compounding). The reason for this is that in each firing of the 3MPT systems, only 2-D images would be reconstructed (e.g., three images for 3MPT-SLA and six images for 3MPT-2MLA), and only the motion during these five compounds could affect these 2-D images. However, in the 9×9 DWC system, full volumes were constructed for every firing, resulting in motion affecting the image reconstruction during all 81 compounds leading to more severe incoherence.

Of course, any motion artifact is directly related to the characteristics of the motion. For example, motion parallel to the transducer surface (i.e., in azimuth or elevation direction) showed to have little impact on any of the beamforming methodologies studied (data not shown). On the other hand, axial motion was detrimental for 9×9 DWC while the other approaches were less affected. In this paper, the axial motion was assumed to be 5 cm/s as a realistic value for myocardial motion. Of course, when higher axial velocities would occur, the deterioration of image quality would increase for all of the methods presented.

The proposed 3MPT imaging systems showed stitching artifacts [see Fig. 9(b) and (h)] as a result of the one-side-to-the-other-side sequential scan scheme in the elevation dimension causing fairly large time lag at the borders of the subsectors simultaneously reconstructed. These artifacts could easily be avoided by adapting the conventional scan

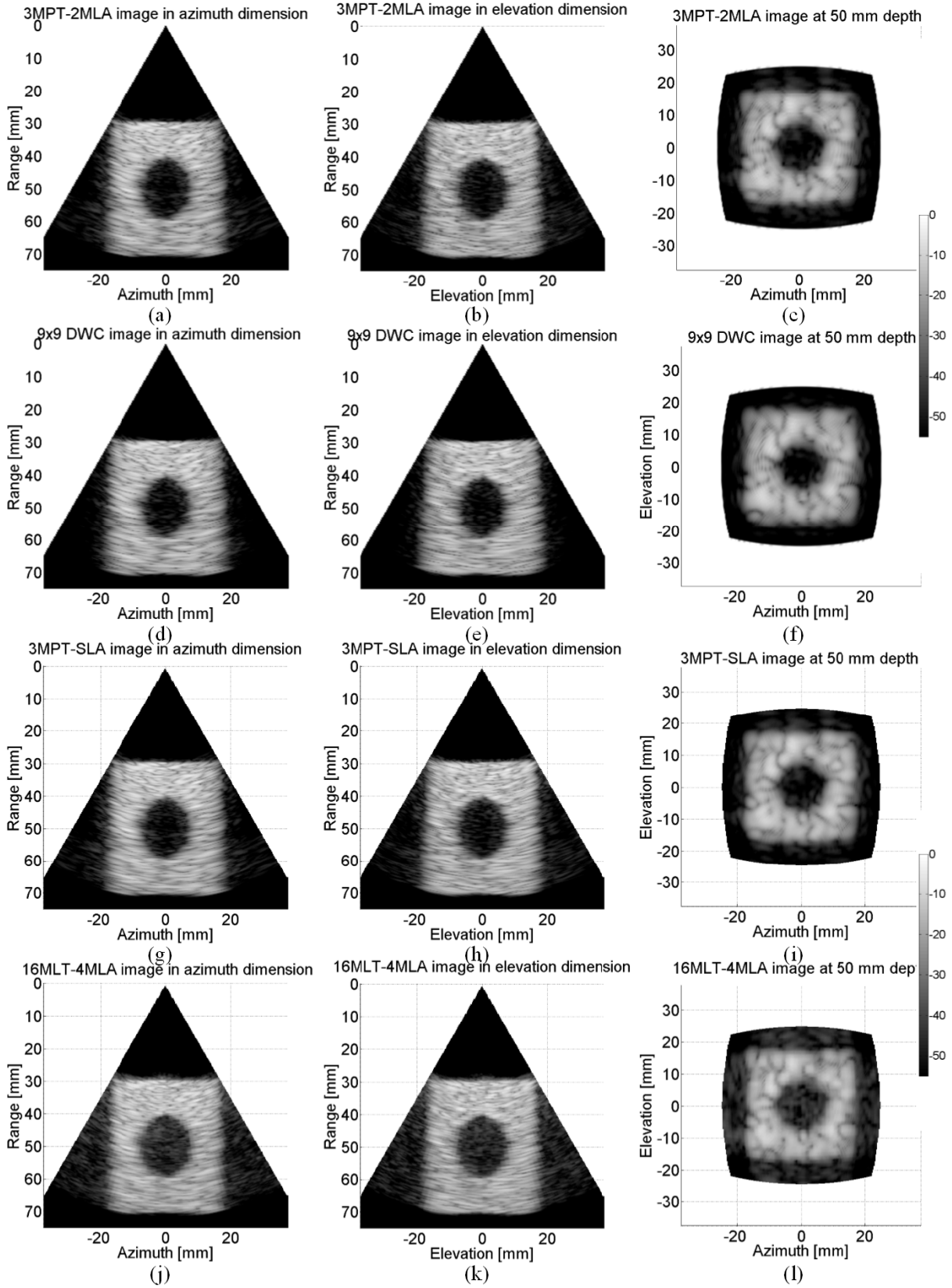

Fig. 7. B-mode images of the static cystic phantom. (a)–(c) Results of the 3MPT-2MLA. (d)–(f) 9×9 DWC. (g)–(i) 3MPT-SLA. (j)–(l) 16MLT-4MLA. Left: 2-D image slice in the azimuth-axial plane. Middle: elevation-axial plane. Right: *C* plane at 50-mm depth. The display dynamic range is -55 dB.

sequence to scan from the subsector edges to the center as this distributes the time lag between recordings of the neighboring lines more evenly as proposed for MLT imaging [15], [17]. Similarly, a modified firing sequence and/or using cross correlation to correct for motion between consecutive recordings have been proposed to limit motion artifacts for 2-D diverging

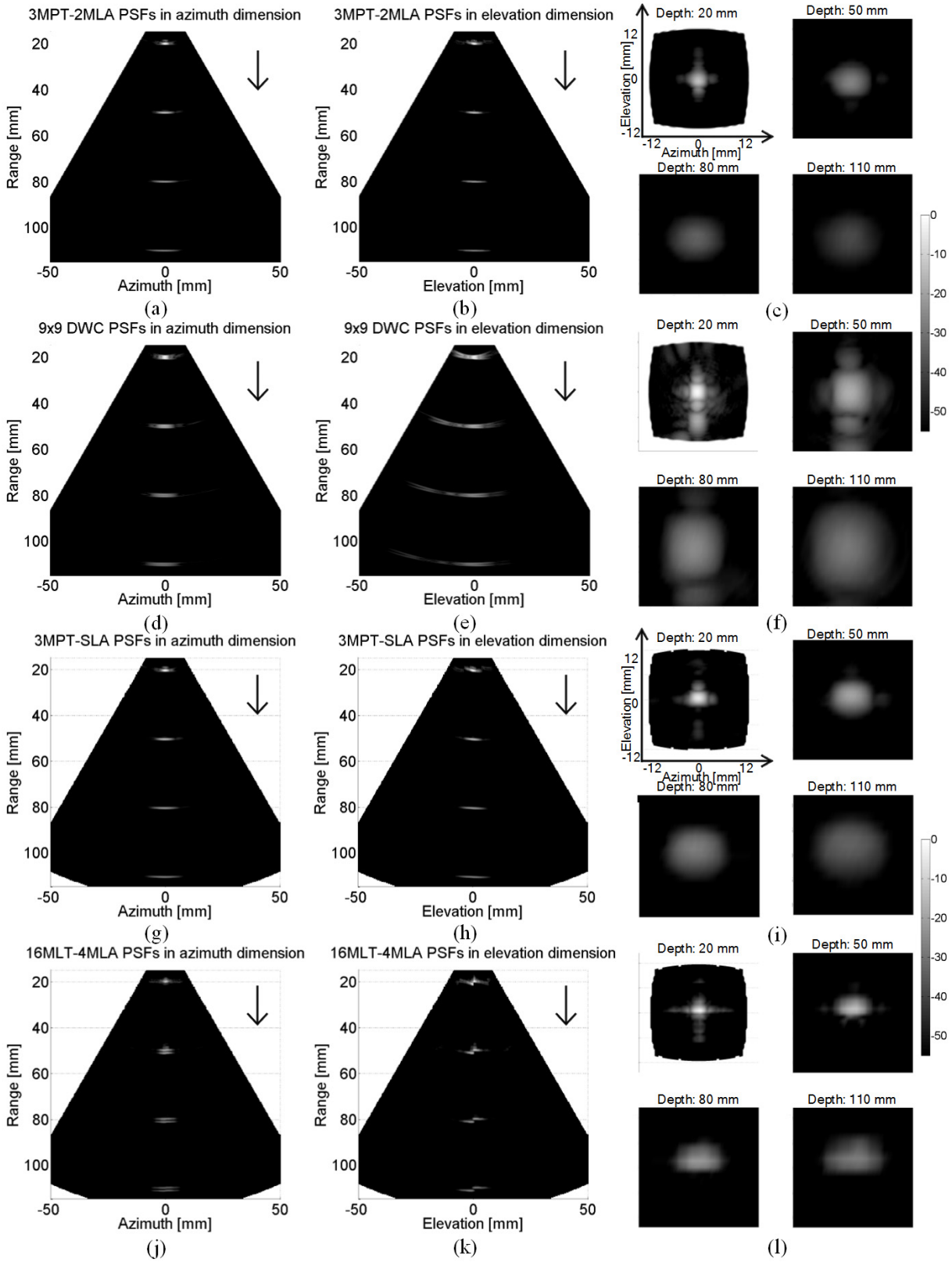

Fig. 8. PSFs of the four imaging systems when the point scatterers moved in the axial direction with the velocity of 5 cm/s. (a)–(c) Results of the 3MPT-2MLA. (d)–(f) 9 × 9 DWC. (g)–(i) 3MPT-SLA. (j)–(l) 16MLT-4MLA. The legend at the top-right corner of images illustrates the motion direction. All the figures in the right column follow the same axes as illustrated in the top-left one. The display dynamic range is −55 dB.

wave compounding [12], [24]–[27]. In this paper, no attempt was made to correct for these motion artifacts in order to compare the intrinsic sensitivity of all systems to motion. In addition, directly extrapolating the 2-D motion-correction techniques to 3-D might not be trivial and is thus outside of the scope of this paper.

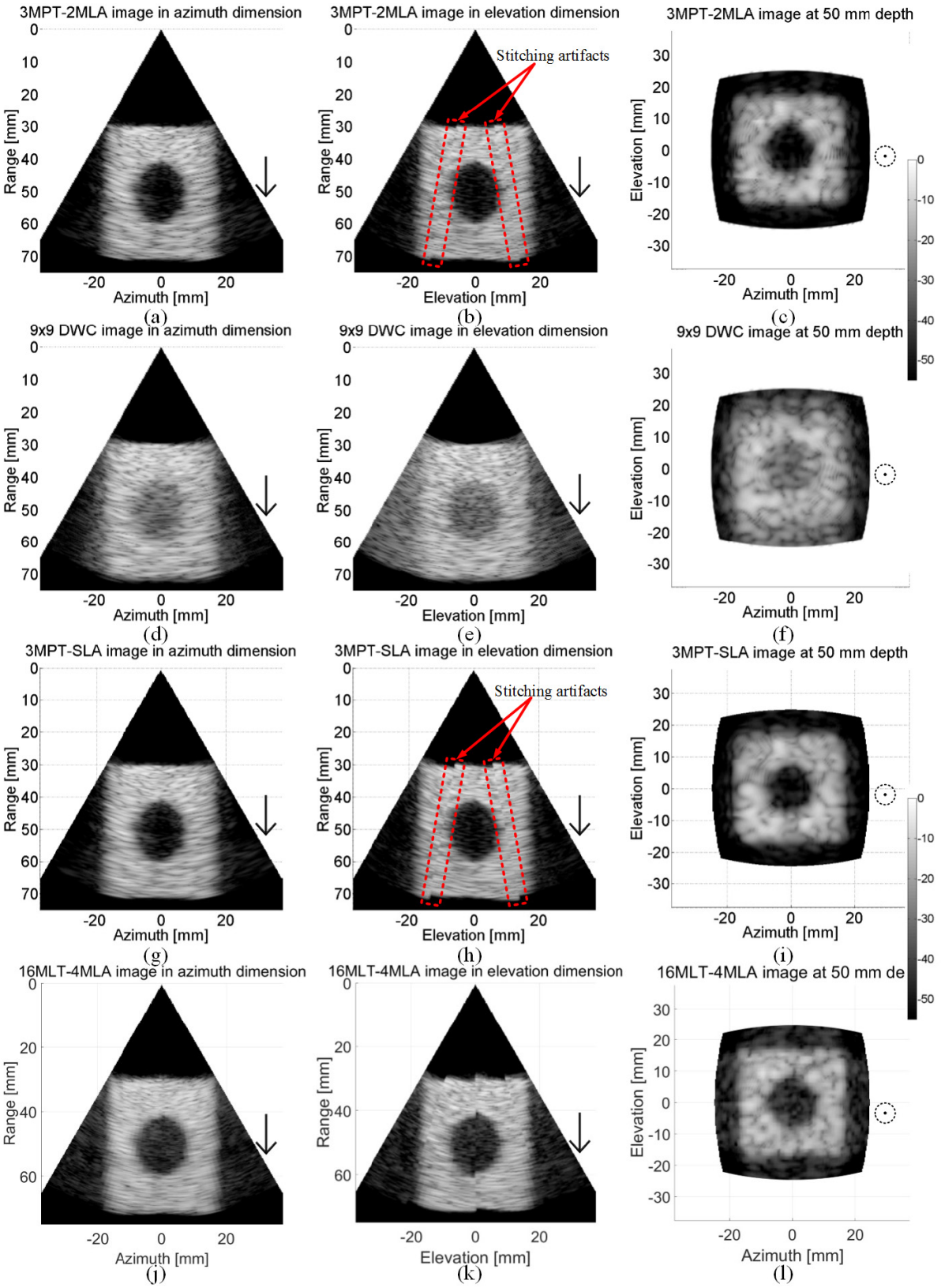

Fig. 9. B-mode images of the cystic phantom with motion of 5 cm/s in the axial direction. (a)–(c) Results of the 3MPT-2MLA. (d)–(f) 9 × 9 DWC. (g)–(i) 3MPT-SLA. (j)–(l) 16MLT-4MLA. Left: 2-D image slice in the azimuth-axial plane. Middle: elevation-axial plane. Right: *C* plane at 50-mm depth. The legend at the top-right corner of images illustrates the motion direction. Red dashed-line box: stitching artifacts. The display dynamic range is −55 dB.

In this context, it is worth pointing out that a limitation of this paper is that we did not try to optimize the different scan sequences for a given application but merely implemented sequences previously described in the literature (i.e., for 9 × 9 DWC and 16MLT-4MLA) as well as two setups of the newly proposed MPT scanning. Although the latter could

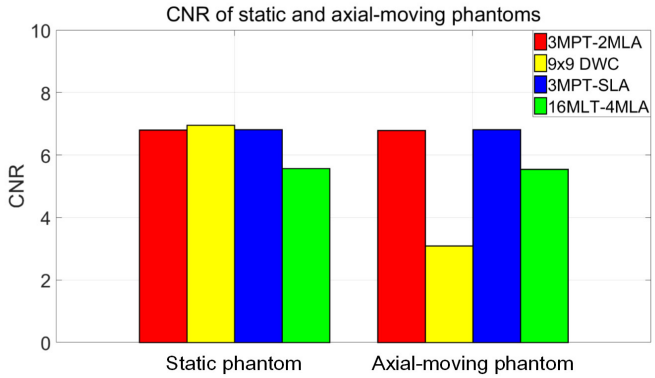

Fig. 10. CNR of the four imaging systems in static and axial-moving states. The quantitative results of the 3MPT-2MLA are [6.80, 6.79], the 9×9 DWC [6.95, 3.09], the 3MPT-SLA [6.81, 6.81], and the 16MLT-4MLA [5.58, 5.54].

also have been implemented for similar volume rates by combining DWC and MLT in another way (e.g., 3DWC-2MLT, 7DWC-4MLT, and 9DWC-5MLT), the current design of 5DWC-3MLT was based on heuristic arguments related to CNR and isotropic image resolution. Nevertheless, further optimizing this newly proposed MPT beam forming approach for a given application remains the topic of future work and fell outside the scope of this initial feasibility study.

It is worth pointing out that an advantage of 3MPT over 3-D diverging wave imaging may be that it better preserves penetration and SNR of the imaging system given that the acoustic energy remains more concentrated in space and that the effective transmit aperture used is larger (see Fig. 2). As fast volumetric imaging is primarily interesting for functional imaging of the heart, motion estimation is essential and sufficient SNR is, therefore, critical to keep the variance in the motion estimates limited.

Finally, although superposition of the different MPT beams in the near field could result in (thermal) bioeffects, solutions similar to the ones proposed for MLT imaging [23] could be used in order to stay within acceptable safety limits.

V. Conclusion

In this paper, a novel beamforming method for volumetric cardiac imaging at high spatial and temporal resolution was proposed by means of simultaneously transmitting multiple planar diverging waves, i.e., MPT imaging. The feasibility of two 3MPT imaging systems was demonstrated and the performance of these systems was compared with a DWC system and a 3-D MLT system through computer simulations. Both the qualitative and quantitative results showed that the 3MPT imaging systems outperformed the DWC system and the MLT system when the frame rate was similar, in particular for moving objects. As a result, MPT imaging could be a valid solution for fast real-time volumetric cardiac imaging. Further optimizations and implementation of this imaging approach on an experimental system are the topic of future work.

References

[1] R. C. Houck, J. Cooke, and E. A. Gill, "Three-dimensional echo: Transition from theory to real-time, a technology now ready for prime time," *Current Problems Diagnostic Radiol.*, vol. 34, no. 3, pp. 85–105, 2005.

[2] R. M. Lang, V. Mor-Avi, L. Sugeng, P. S. Nieman, and D. J. Sahn, "Three-dimensional echocardiography: The benefits of the additional dimension," *J. Amer. College Cardiol.*, vol. 48, no. 10, pp. 2053–2069, 2006.

[3] S. Brekke *et al.*, "Volume stitching in three-dimensional echocardiography: Distortion analysis and extension to real time," *Ultrasound Med. Biol.*, vol. 33, no. 5, pp. 782–796, 2007.

[4] D. P. Shattuck, M. D. Weinshenker, S. W. Smith, and O. T. von Ramm, "Explososcan: A parallel processing technique for high speed ultrasound imaging with linear phased arrays," *J. Acoust. Soc. Amer.*, vol. 75, no. 4, pp. 1273–1282, 1984.

[5] G. Montaldo, M. Tanter, J. Bercoff, N. Benech, and M. Fink, "Coherent plane-wave compounding for very high frame rate ultrasonography and transient elastography," *IEEE Trans. Ultrason., Ferroelect., Freq. Control*, vol. 56, no. 3, pp. 489–506, Mar. 2009.

[6] M. Couade *et al.*, "Ultrafast imaging of the heart using circular wave synthetic imaging with phased arrays," in *Proc. IEEE Int. Ultrason. Symp. (IUS)*, Sep. 2009, pp. 515–518.

[7] C. Papadacci, M. Pernot, M. Couade, M. Fink, and M. Tanter, "High-contrast ultrafast imaging of the heart," *IEEE Trans. Ultrason., Ferroelect., Freq. Control*, vol. 61, no. 2, pp. 288–301, Feb. 2014.

[8] H. Hasegawa and H. Kanai, "High-frame-rate echocardiography using diverging transmit beams and parallel receive beamforming," *J. Med. Ultrason.*, vol. 38, no. 3, pp. 129–140, 2011.

[9] J. Provost *et al.*, "3D ultrafast ultrasound imaging *in vivo*," *Phys. Med. Biol.*, vol. 59, no. 19, pp. L1–L13, 2014.

[10] J. L. Gennisson *et al.*, "4-D ultrafast shear-wave imaging," *IEEE Trans. Ultrason., Ferroelect., Freq. Control*, vol. 62, no. 6, pp. 1059–1065, Jun. 2015.

[11] J. Wang and J. Y. Lu, "Motion artifacts of extended high frame rate imaging," *IEEE Trans. Ultrason., Ferroelect., Freq. Control*, vol. 54, no. 7, pp. 1303–1315, Jul. 2007.

[12] B. Denarie *et al.*, "Coherent plane wave compounding for very high frame rate ultrasonography of rapidly moving targets," *IEEE Trans. Med. Imag.*, vol. 32, no. 7, pp. 1265–1276, Jul. 2013.

[13] R. Mallart and M. Fink, "Improved imaging rate through simultaneous transmission of several ultrasound beams," *Proc. SPIE*, vol. 1733, pp. 120–130, Nov. 1992.

[14] L. Tong, H. Gao, and J. D'hooge, "Multi-transmit beam forming for fast cardiac imaging-a simulation study," *IEEE Trans. Ultrason., Ferroelect., Freq. Control*, vol. 60, no. 8, pp. 1719–1731, Sep. 2013.

[15] L. Tong, A. Ramalli, R. Jasaityte, P. Tortoli, and J. D'hooge, "Multi-transmit beam forming for fast cardiac imaging-experimental validation and *in vivo* application," *IEEE Trans. Med. Imag.*, vol. 33, no. 6, pp. 1205–1219, Jun. 2014.

[16] L. Tong, A. Ortega, H. Gao, and J. D'hooge, "Fast three-dimensional ultrasound cardiac imaging using multi-transmit beam forming: A simulation study," in *Proc. IEEE Int. Ultrason. Symp. (IUS)*, Sep. 2013, pp. 1456–1459.

[17] B. Denarie, T. Bjastad, and H. Torp, "Multi-line transmission in 3-D with reduced crosstalk artifacts: A proof of concept study," *IEEE Trans. Ultrason., Ferroelect., Freq. Control*, vol. 60, no. 8, pp. 1708–1718, Aug. 2013.

[18] A. Ortega *et al.*, "A comparison of the performance of different multiline transmit setups for fast volumetric cardiac ultrasound," *IEEE Trans. Ultrason., Ferroelect., Freq. Control*, vol. 63, no. 12, pp. 2082–2091, Dec. 2016.

[19] A. Ortega, L. Tong, P. Santos, B. Heyde, and J. D'hooge, "Fast volumetric cardiac ultrasound: A comparison of different multi-line transmit setups by computer simulation," in *Proc. IEEE Int. Ultrason. Symp. (IUS)*, Sep. 2014, pp. 1195–1198.

[20] J. A. Jensen, "FIELD: A program for simulating ultrasound systems," in *Proc. IEEE 10th Nordic-Baltic Conf. Biomed. Imag.*, vol. 34. Mar. 1996, pp. 351–353.

[21] L. Demi, M. D. Verweij, and K. W. Van Dongen, "Parallel transmit beamforming using orthogonal frequency division multiplexing applied to harmonic imaging-a feasibility study," *IEEE Trans. Ultrason., Ferroelect., Freq. Control*, vol. 59, no. 11, pp. 2439–2447, Nov. 2012.

[22] T. Misaridis and J. A. Jensen, "Use of modulated excitation signals in medical ultrasound. Part III: High frame rate imaging," *IEEE Trans. Ultrason., Ferroelect., Freq. Control*, vol. 52, no. 2, pp. 208–219, Feb. 2005.

[23] B. Madore, P. J. White, K. Thomenius, and G. T. Clement, "Accelerated focused ultrasound imaging," *IEEE Trans. Ultrason., Ferroelect., Freq. Control*, vol. 56, no. 12, pp. 2612–2623, Dec. 2009.

[24] M. Karaman and M. O'Donnell, "Adaptive multi-element synthetic aperture imaging with motion and phase aberration correction," *IEEE Trans. Ultrason., Ferroelect., Freq. Control*, vol. 45, no. 4, pp. 1077–1087, Apr. 1998.
[25] N. Oddershede and J. A. Jensen, "Effects influencing focusing in synthetic aperture vector flow imaging," *IEEE Trans. Ultrason., Ferroelect., Freq. Control*, vol. 54, no. 9, pp. 1811–1825, Sep. 2007.
[26] K. S. Kim, J. S. Hwang, J. S. Jeong, and T. K. Song, "An efficient motion estimation and compensation method for ultrasound synthetic aperture imaging," *Ultrason. Imag.*, vol. 24, no. 2, pp. 81–99, Feb. 2002.
[27] B. Yiu, I. K. Tsang, and A. C. Yu, "A modified synthetic aperture imaging approach with axial motion compensation," in *Proc. IEEE Int. Ultrason. Symp. (IUS)*, Sep. 2008, pp. 1254–1257.

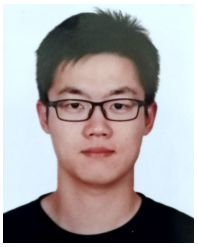

Yinran Chen was born in Fujian, China, in 1991. He received the bachelor's degree in biomedical engineering from Tsinghua University, Beijing, China, in 2014, where he is currently pursuing the Ph.D. degree with the Department of Biomedical Engineering.

He joined the Cardiovascular Imaging and Dynamics Laboratory, University of Leuven, Leuven, Belgium, as a Visiting Scholar, in 2015. His current research interests include ultrasonics beamforming and signal processing for high-frame-rate imaging.

Ling Tong (S'11–M'14) was born in Hebei, China, in 1983. She received the bachelor's degree in physics from Hebei University, China, in 2006, the master's degree in condensed matter physics from Peking University, China, in 2009, and the Ph.D. degree from the Department of Cardiovascular Sciences, University of Leuven (KU Leuven), Belgium, in 2013.

From January 2014 to August 2016, she worked as a Post-Doctoral Researcher with the Department of Biomedical Engineering, Tsinghua University, Beijing, China. She is currently working for Supersonic Imagine, S.A. Her main research field is ultrasound beamforming and signal processing for high-frame-rate cardiac imaging.

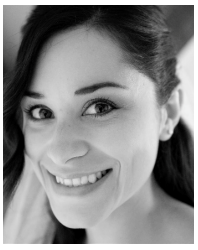

Alejandra Ortega (S'11) was born in Medellin, Colombia, in 1988. She received the bachelor's degree in biomedical engineering from the Antioquia School of Engineering, Envigado, Colombia, in 2011. She is currently pursuing the Ph.D. degree with the Cardiovascular Imaging and Dynamics Laboratory, Katholieke Universiteit Leuven, Leuven, Belgium.

She integrated the Biomedical Engineering Research Group EIA-CES (GIBEC), with an emphasis on medical imaging. She was an Intern with the Magnetic Resonance Elastography Laboratory, Mayo Clinic, Rochester, MN, USA. Her current research interests include ultrasound beamforming for cardiac imaging.

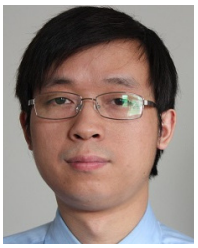

Jianwen Luo (S'02–M'06–SM'14) received the B.S. and Ph.D. (Hons.) degrees in biomedical engineering from Tsinghua University, Beijing, China, in 2000 and 2005, respectively.

He was a Postdoctoral Research Scientist from 2005 to 2009 and an Associate Research Scientist from 2009 to 2011 with the Department of Biomedical Engineering, Columbia University, New York City, NY, USA. He joined the Department of Biomedical Engineering, Tsinghua University, as a Professor, in 2011. He has authored or coauthored over 110 papers in international journals, 50 conference proceedings papers, and 120 conference abstracts. His current research interests include ultrasound imaging and fluorescence molecular imaging.

Dr. Luo was enrolled in the Thousand Young Talents Program of China in 2012, and received the Excellent Young Scientists Fund from the National Natural Science Foundation of China in 2013. He was supported by the Young Scientists Project of the National Key Research and Development Program of China in 2016. He serves as an Advisory Editorial Board Member of the *Journal of Ultrasound in Medicine*, and a member of the IEEE Engineering in Medicine and Biology Society Technical Committee on Biomedical Imaging and Image Processing.

Jan D'hooge (M'98) was born in Sint-Niklaas, Belgium, in 1972. He received the M.Sc. and Ph.D. degrees in physics from the University of Leuven, Leuven, Belgium, in 1994 and 1999, respectively. His dissertation was focused on the interaction of ultrasonic waves and biological tissues by means of computer simulation.

He was a Post-Doctoral Researcher with the Medical Imaging Computing Laboratory, University of Leuven, where he became acquainted with general problems in medical imaging, such as elastic registration, segmentation, shape analysis, and data acquisition problems related to other modalities, particularly in MRI. In 2006, he joined the Department of Cardiovascular Diseases with the Medical Faculty, Katholieke Universiteit Leuven, Leuven, as an Associate Professor. Since 2009, he has been a part-time Visiting Professor with the Norwegian Institute of Science and Technology, Trondheim, Norway. He has coauthored over 150 peer-reviewed papers, contributed to eight books, and coedited one book. His current research interests include myocardial tissue characterization, deformation imaging, and cardiac patho-physiology.

Dr. D'hooge is a member of the Acoustical Society of America and the European Association of Echocardiography. In 1999, he was a recipient of the Young Investigator Award of the Belgian Society of Echocardiography. In 2000, he was nominated for the Young Investigator Award of the European Society of Echocardiography. He was the Chair of the Ultrasound Conference of the SPIE Medical Imaging Symposium from 2008 to 2011, the Technical Vice-Chair of the IEEE Ultrasonics Symposium from 2008 to 2012, and the Technical Chair of the IEEE Ultrasonics Symposium in 2014. He was an elected AdCom Member of the IEEE-UFFC Society from 2010 to 2012.